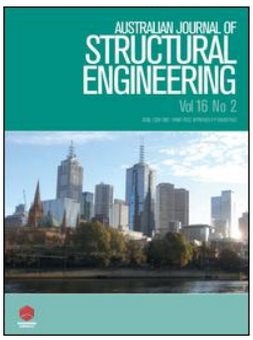

Australian Journal of Structural Engineering

ISSN: (Print) (Online) Journal homepage: https://engineersaustralia.tandfonline.com/loi/tsen20

New analytical method for computing moment redistribution in RC beams under concentrated load

Mohamed A. Farouk & Khaled F. Khalil

To cite this article: Mohamed A. Farouk & Khaled F. Khalil (2021): New analytical method for computing moment redistribution in RC beams under concentrated load, Australian Journal of Structural Engineering, DOI: 10.1080/13287982.2021.1912518

To link to this article: https://doi.org/10.1080/13287982.2021.1912518

AUSTRALIAN JOURNAL OF STRUCTURAL ENGINEERING
https://doi.org/10.1080/13287982.2021.1912518

Taylor & Francis
Taylor & Francis Group

ARTICLE

New analytical method for computing moment redistribution in RC beams under concentrated load

Mohamed A. Farouk[a] and Khaled F. Khalil[b#]

[a]Civil Engineering Department, Delta University, Egypt; [b]Civil Engineering Department, Zagazig University, Zagazig, Egypt

ABSTRACT

Computing the moments in RC structures after the yield by linear elastic analysis can lead to an inaccurate assessment of the behaviour due to the nonlinear behaviour. Therefore, it can become necessary to use more advanced methodologies to achieve a higher degree of performance optimisation of structures than those resulting from the simplified approaches adopted by existing design codes based on linear elastic analysis with redistribution of internal forces. The moment redistribution is supposed to start after occurring the cracks of concrete, but with small ratio. In this study, the moment redistribution before the yielding will be neglected, and the redistribution is focused after the yield. This paper suggests a mathematical model to investigate the moment redistribution in RC beams after yielding analytically. In the suggested mathematical model, the beam after forming the plastic hinges is converted into a virtual beam that can be analysed by structural linear analysis. The plastic hinges in the virtual beam will be represented as rotational springs having a linear rotational stiffness against the induced moment. The actual moments can be found through derived relationships in the mathematical model between it and the virtual moment. The mathematical model was verified and it gave values of moment matching experimental results. Also, a comparison for degree of moment redistribution among the suggested mathematical model and several design codes was performed. The analytical results indicate that the proposed mathematical model can be used for analysis of moment redistribution of RC beams.

KEYWORDS

Moment redistribution; plastic hinge and mathematical model

1. Introduction

Moment redistribution is dependent on adequate ductility in plastic hinge regions. Plastic hinge regions develop at sections of maximum positive or negative moment and cause a shift in the elastic moment diagram. The usual result is a reduction in the values of maximum negative moments in the support regions and an increase in the values of positive moments between supports from those computed by elastic analysis.

However, because negative moments are determined for one loading arrangement and positive moments for another, economies in reinforcement can sometimes be realised (depending on the load pattern) by reducing maximum elastic positive moments and increasing negative moments, thus narrowing the envelope of maximum negative and positive moments at any section in the span. The plastic hinges permit the utilisation of the full capacity of more cross-sections of a flexural member at ultimate loads **(ACI – 318-19)**.

The primary experiments regarding the moment redistribution in continuous reinforced concrete beams had been achieved by Mattock (1959) **and** Cohn (1964). Their works indicated that the redistribution of the design bending moments up to 25% does not appreciably change the curvature and the crack widths in a continuous RC beam designed by using the elastic theory. Scholz (1993) investigated and verified the influence of the various beam slenderness and stiffness on the moment redistribution in continuous RC beams using the ductility concept. He compared his proposed approach with the allowable moment redistribution given within the Canadian code, and concluded that his approach predicts greater realistic results for moment redistribution in comparison to the results of the Canadian code. **Lin and Chien (**Lin and Chien 2002) studied the effect of longitudinal and transverse reinforcement on the ductility and moment redistribution of 26 continuous RC beams. They concluded that the transverse reinforcements confine the concrete and increase the ductility and moment redistribution in the continuous flexural members. In continuous concrete members, moment redistribution may take place with the primary crack initiation and its evolution may be influenced by some phases such as the formation of plastic hinges at critical sections (Lou, Lopes, and Lopes 2013). The authors have recently conducted a numerical investigation into redistribution of moments in two-span continuous reinforced NSC and HSC beams (Lou, Lopes, and Lopes 2014b). There are many parameters that may affect notably the ductility and moment redistribution

CONTACT Mohamed A. Farouk moh.anour@yahoo.com
[#]*Professor of Reinforced Concrete Structures, email: drmoh.anwar@yahoo.com*

in concrete members (Kodur and Campbell 1999; Lou, Lopes, and Lopes 2014c). Of these parameters, the transverse reinforcement or the resulting confinement has been recognised as an important parameter (Sheikh, Laine, and Cui 2013). According to the standards for concrete structures, such as **the Eurocode (2004), American standard [2018] and Canadian standard (2004)**, it is permissible to make use of linear elastic analysis with limited moment redistribution for continuous reinforced concrete beams at the ultimate limit state, without an explicit check of the structural ductility. However, the allowable moment redistribution varies slightly between standards. In the Eurocode and Canadian standards, the allowable moment redistribution is a function of the ratio of the depth of compression and the effective depth, c/d, whilst according to the American standard, the moment redistribution is a function of the strain in the tensile reinforcement. Additionally, the Eurocode accounts for the concrete class through two separate equations for normal-strength concrete ($f_{ck} \leq 50$ MPa) and high-strength concrete (f_{ck}> 50 MPa). In order to ensure sufficiently safe moment redistribution, the degree of moment redistribution is limited to 30% in the Eurocode and 20% in the American and Canadian standards. The upper limit according to the Eurocode is valid for structures with longitudinal reinforcing steel in ductility class B ($1.08 \leq f_t/f_y$ and $5.0\% \leq \varepsilon_{su}$) or class C ($1.1 \leq f_t/f_y$<1.35 and $7.5\% \leq \varepsilon_{su}$), whilst the degree of moment redistribution is limited to 20% in steel ductility class A ($1.05 \leq f_t/f_y$and $2.5\% \leq \varepsilon_{su}$). The percentage degree of moment redistribution can be calculated using **Eqs. (1) -(2)** for the Eurocode, **Eq. (3)** for the American standard and **Eq. (4)** for the Canadian standard:

$$\eta = 56 - 125(0.6 + \frac{0.0014}{\varepsilon_{cu}})\frac{c}{d}f_{ck} \leq 50Mpa \textbf{(1)}$$

$$\eta = 46 - 125(0.6 + \frac{0.0014}{\varepsilon_{cu}})\frac{c}{d}f_{ck} > 50Mpa \textbf{(2)}$$

$$\eta = 1000\varepsilon_s \textbf{(3)} \eta = 30 - 50\frac{c}{d} \textbf{(4)}$$

where $\varepsilon_{cu}$is the concrete compressive ultimate strain, f_{ck} is the concrete compressive characteristic strength, c is the neutral axis depth, d is the effective cross-section depth and ε_s is the longitudinal tensile reinforcement strain. According to the American standard, the reinforcement tensile strain is required to be $\geq 0.75\%$ to allow moment redistribution to take place. In Figure 1, the allowable degree of moment redistribution is illustrated for the three standards for normal-strength concrete and steel ductility class B or C. Available moment redistribution in reinforced concrete structures is influenced by several factors, with the available plastic rotation capacity of critical regions identified as the most important factor, CEB-FIP (1998). Further, the plastic rotation capacity depends on factors related to material, structure and loading. The main factors for linear elements subjected to such moment redistribution are the concrete strength, the reinforcing steel strength and ductility, the interaction between reinforcing steel and concrete, the size and shape of the cross-section, the tensile and compression reinforcement ratio, the shear reinforcement ratio, detailing of the reinforcement, the slenderness ratio and, moreover, the static system, and associated load characteristics.

To ensure sufficient plastic rotation capacity, and thus to determine the capacity for moment redistribution, a numbers of models with various levels of complexity can be used, **CEB-FIP** (CEB-FIP 1998). Generally, the more complex models are based on the definition of the moment–curvature relationship or the moment–rotation relationship, whilst simpler models are based on graphs of the plastic rotation capacity. For instance, **the Eurocode (2009)** proposes a graphical model for estimating available plastic rotation capacity as a function of the ratio between concrete compressive depth and sectional effective depth, ductility of reinforcing steel, concrete characteristics

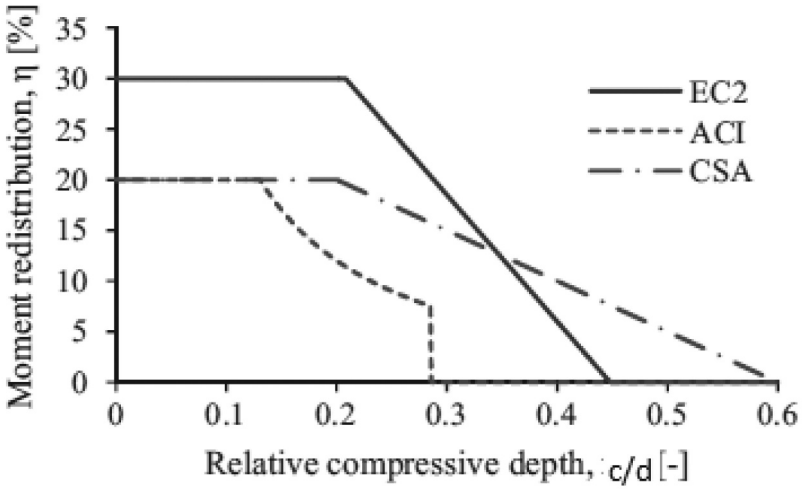

Figure 1. Allowable moment redistribution for continuous reinforced concrete beams according to Eurocode (EC2), American standard (ACI) and Canadian standard (CSA).

and shear slenderness. Advanced analysis of the structural ductility can also be carried out using nonlinear finite element analysis, as described in work such as Rodrigues EA *et al* (2013), Gamino AL *et al* (2007).

2. Analytical solution

2.1. The materials modelling

i. Concrete constitutive model

The concrete constitutive model in the analytical solution will be represented as shown in Figure 2, the first part is ascending branch and will be represented as in Eq. (5) proposed by Saenz (1965)

$$\sigma = \frac{E_0 \varepsilon}{1 + (\frac{E_0}{E_{sc}} - 2)(\frac{\varepsilon}{\varepsilon_{max}}) + (\frac{\varepsilon}{\varepsilon_{max}})^2} \tag{5}$$

Where: E_{sc} is the secant modulus of elasticity at the peak stress, E_0 is the initial modulus of elasticity and ε_{max} is the strain at peak stress. The stress in the second part of the curve is assumed to be constant with increasing the strain.

ii. Reinforcement steel modelling

The reinforcement steel will be modelled as an elastic strain-hardening material as shown in Figure 3

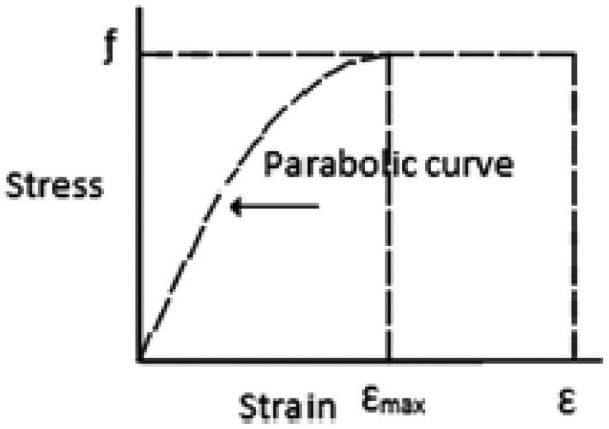

Figure 2. Concrete modelling.

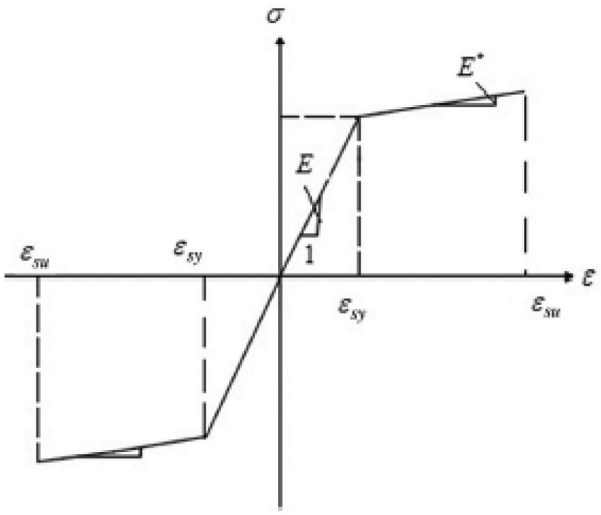

Figure 3. Reinforcement steel modelling.

2.2. The curvature after yielding

By using the shown stress and strain distribution over RC section in Figure 4, Mohamed A. Farouk and Khaled F. Khalil (2020) based on analytical solution presented the following relationships which are useful in the current study:

$$c = \frac{-\xi + \sqrt{\xi^2 - 4\lambda\psi}}{2\lambda} \tag{6}$$

where

$$\xi = (A_s' f_s' + A_s(\varepsilon_c E^* - f_y + E^* \varepsilon_y)) \tag{7}$$

$$\psi = -A_s E^* \varepsilon_c d \tag{8}$$

$$\lambda = \frac{\varphi b}{2}(\sigma + 2\sum_{N=0.1}^{0.9}(\sigma_N)) \tag{9}$$

Where: N = 0.1, 0.2, 0.3, … .0.9, φ is the ratio of segment height to the depth of neutral axis from compression fibre (c), in the current analysis φ is assumed to equal to 0.1.

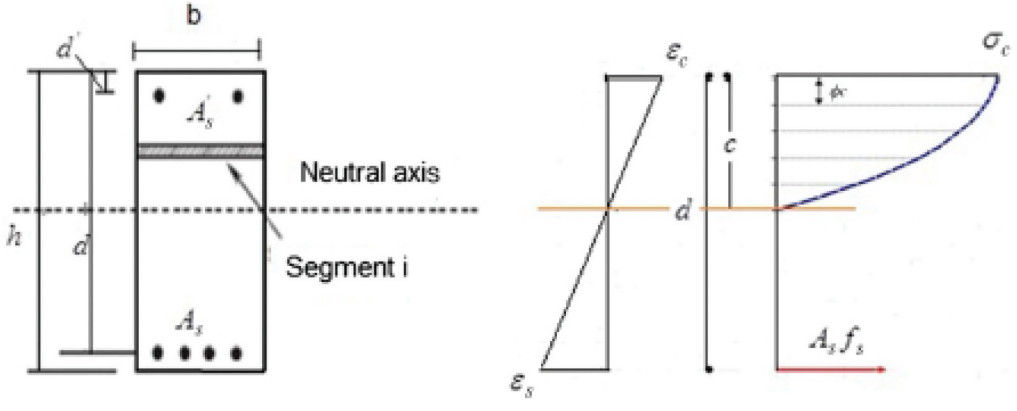

Figure 4. Stress and strain distribution of a reinforced concrete section.

The bending moment which is corresponded to the assumed value of concrete strain can be calculated as follows:

(10)

The bending moment can be formulated as

$$M = \frac{\varphi b c^2}{2}\left[\sigma(1-0.5\varphi) + \sum_{N=0.1}^{0.9}(2\sigma_n(1-10N\varphi)\right] + A_s^{'}f_s^{'}(d-d^{'}) \tag{11}$$

The curvature at any stage of loading after the yield can be calculated as the following equation

$$\phi = \frac{\varepsilon_c}{c} \tag{12}$$

At the ultimate moment

$$\phi_u = \frac{\varepsilon_{cu}}{c_u} \tag{13}$$

where ε_{cu}: the concrete strain at ultimate moment.

c_u: the depth of compression zone at ultimate moment

At the yield moment

$$\phi_y = \frac{\varepsilon_{cy}}{c_y} \tag{14}$$

where ε_{cy}: the concrete strain at yield moment

c_y: the depth of compression zone at yield stage can be calculated based on linear analysis by solving the following equation

$$\frac{b}{2}c_y^2 + n(A_s - A_s^{'})c_y - n(A_s^{'}d^{'} + A_s d) = 0 \tag{15}$$

where n: the modular ratio

$$\varepsilon_{cy} = \varepsilon_{sy}\frac{c_y}{d-c_y} \tag{16}$$

2.3. Simplified equation for computing plastic rotation capacity

For the shown cantilever beam in Figure 5, the total rotation (θ_{total}) over the beam length can be divided into elastic (θ_{el}) and plastic (θ_{pl}) rotations. The plastic hinge rotation (θ_{pl}) on each side of the critical section can be defined as:

$$\theta_p = \int_0^{l_y}(\phi(x) - \phi_y).dx \tag{17}$$

In which, $l_y$is the beam length over which the bending moment is larger than the yielding moment (My) or the distance between the critical section and the location where tension steel bars start yielding and $\phi(x)$is the curvature at a distance x from the critical section at the ultimate load stage.

Mohamed A. Farouk and Khaled F. Khalil (2020) analysed five simply supported beams under middle concentrated load with varying the steel reinforcement ratio in-between (0.0074 to 0.0294), to compute the plastic hinge rotation. They concluded that the relationship between the moment and curvature after the yield can be considered linearly as shown in Figure 6. This means the curvature takes the same shape of the bending moment. As a result, the curvature through the yield length also can be assumed linear as shown in Figure 7.

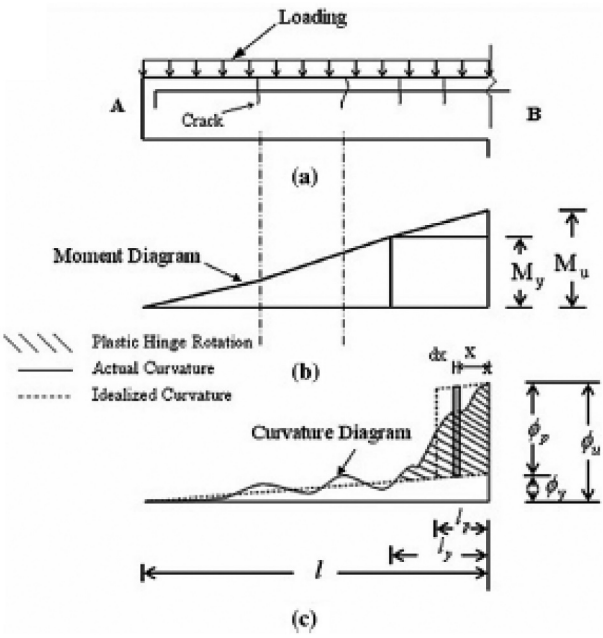

Figure 5. The curvature and the bending moment of cantilever beam.

Thus, the equation of computing the plastic rotation at the ultimate moment can be simplified as follows:

$$\theta_{pu} = \frac{1}{2}(\phi_u - \phi_y)l_y \tag{18}$$

l_y depends on the loading type, in the present case, $l_y = \frac{M_u - M_y}{M_u}$

$$\theta_{pu} = \frac{L}{4}(\phi_u - \phi_y)\frac{M_u - M_y}{M_u} \tag{19}$$

2.4. The relationship between a virtual moment and the plastic rotation

The curvature will be assumed linear through the loading after yielding till the ultimate, this is because as mentioned before that the curvature will take the same shape of the moment which will be linear till the ultimate. So, the plastic rotation at any stage of loading can be formulated generally as

$$\theta_p = \frac{1}{2}(\phi - \phi_y).l_y \tag{20}$$

Whereϕ: the curvature of middle section at any step of loading

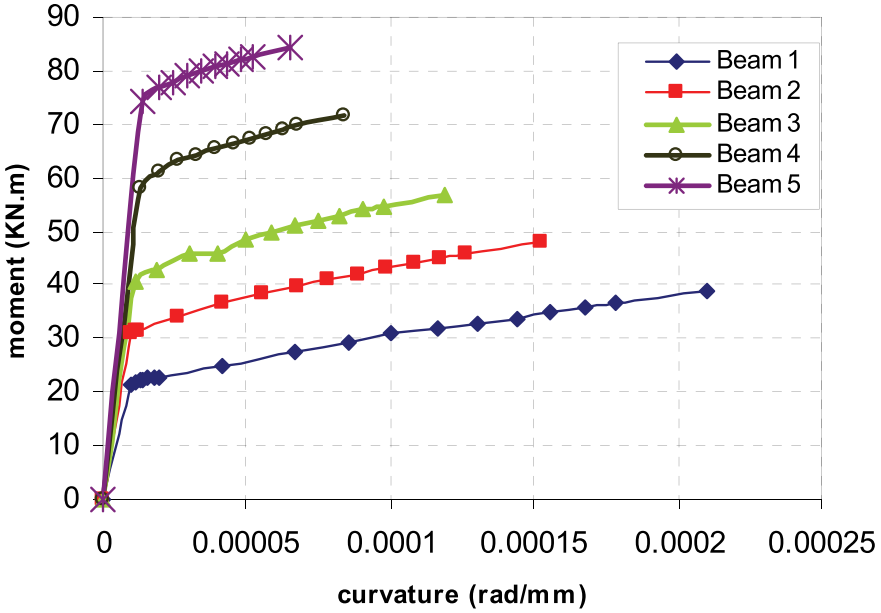

Figure 6. The moment–curvature relationship of the analysed beams.

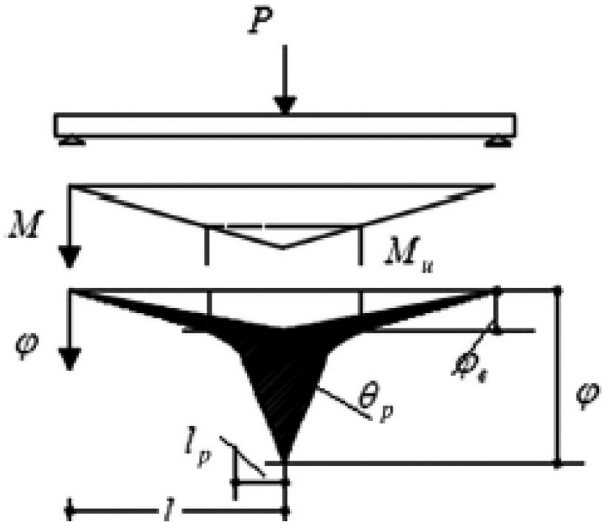

Figure 7. The moment–curvature relationship of the analysed beams.

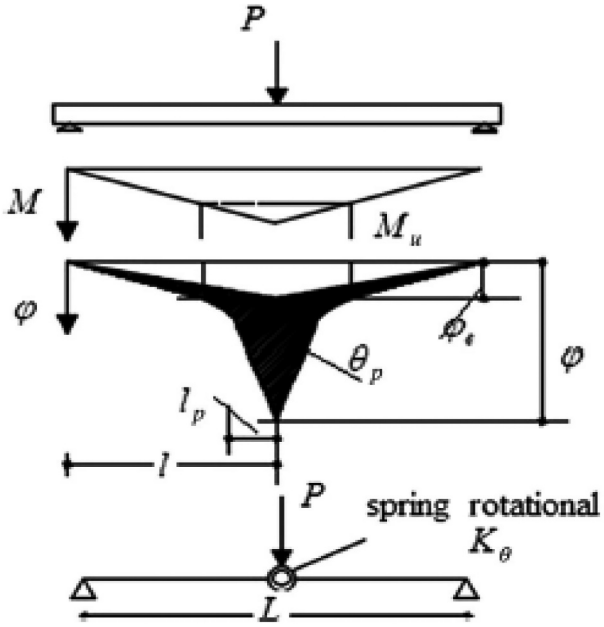

Figure 8. Modelling of yielding zone.

$$l_y = \frac{(M - M_y)}{Q} = \Delta M / \frac{p}{2} \tag{21}$$

M is the bending moment of the middle section at any step of loading, Q is shearing force at yield section. Eq. (20) can be rewritten as

$$\theta_p = \frac{1}{2}(\phi - \phi_y)\frac{\Delta M}{p/2} \tag{22}$$

By using Eq. (22), the plastic rotation at any loading step can be easy computed, not only at the failure stage. The relationship between θ_p and ΔM in Eq. (22) is nonlinear relationship, it is possible to obtain on a linear relationship between the plastic rotation and another moment as follows:

Figure 6 shows the relationship between the moment and curvature of the previous analysed beams (1,2,3,4 and 5), it was clearly observed that

$$\frac{\phi - \phi_y}{M - M_y} = \frac{\phi_u - \phi_y}{M_u - M_y} = const. \tag{23}$$

By multiplying the right side of Eq. (22) by $\Delta ML/\Delta ML$, the equation can be rewritten as

$$\theta_p = \frac{L}{2}\frac{(\phi - \phi_y)}{\Delta M} \cdot \frac{\Delta M^2}{pL/2} \tag{24}$$

By substituting Eq. (23) in Eq. (24), the last equation becomes as

$$\theta_p = \frac{L}{2}\frac{(\phi_u - \phi_y)}{\Delta M_u}.\frac{\Delta M^2}{pL/2} \quad (25)$$

It can be put $const. = \frac{1}{K_\theta} = \frac{L}{2}.\frac{(\phi-\phi_y)}{(M-M_y)}$ **(26)**

And

$$M^* = \frac{\Delta M^2}{PL/2} \quad (27)$$

The plastic rotation capacity at any loading step can be rewritten as

$$\theta_p = \frac{M^*}{K_\theta} \quad (28)$$

Eq. (35) shows a linear relationship between the plastic rotation and a virtual moment. By using this relationship, the RC beam can be modelled as a virtual beam after yielding by representing the plastic zone as intermediate hinge with rotational spring as shown in Figure 8 and Figure 9. This spring has a rotational stiffness$K_\theta$which can be computed based on **Eq.(26)**. M* is the induced moment in the virtual beam that fits linearly with the plastic rotation. The main purpose of converting the original beam to virtual beam, where a virtual moment fits linearly with the plastic rotation is obtaining the moments in indeterminate beams after the yield as the shown in the next section.

3. Mathematical model to compute the moment redistribution in continuous R.C beams under concentrated load

The concept of the suggested mathematical model for computing the moment redistribution after the yield, that converting the original beam to a virtual beam which can be analysed by the linear analysis. In the virtual beam, the plastic zones will be represented as a pin connection with rotational spring (K_θ)that can be deduced as in **Eq. (26)**. The applied load in the virtual beam is the difference between the actual load on the original beam and the yield load. After obtaining the virtual moment at the rotational spring (M*) by using one of the linear structural analysis methods, the actual moment at the plastic zones will be computed based on the relationship between it and the virtual moment such as in Eq. (27). In the current analysis, the cracks will be assumed that spread in the most of the beam between the plastic zones. Thus, the flexural rigidity (EI) of the beam which is used in the linear analysis will be considered as (E_cI_{cr}), where the elastic modulus concrete is according to **ACI** (2019) ($E_c = 4700\sqrt{f_c'}$ N/mm^2), and (I_{cr})is the cracking modulus of inertia. A continuous beam as shown in Figure 10 will be studied to illustrate the concept of the mathematical model.

3.1 The virtual beam and Stiffness of the rotational springs for continuous beam under concentrated load

As mentioned before that the relationship between the moment after yielding and the curvature can be assumed linear, thus the curvature through the yield length can be assumed linear as well. As a result, the plastic rotation can be computed by Eq.(27).

If the yield occurs at the negative moment zone as shown in Figure 9, $l_y$can be determined as

$$M_{-ve} - M_y = \Delta M_{-ve} = Q.l_y \quad (29)$$

$$Q = \frac{p}{2} + \frac{M_{-ve}}{L} \quad (30)$$

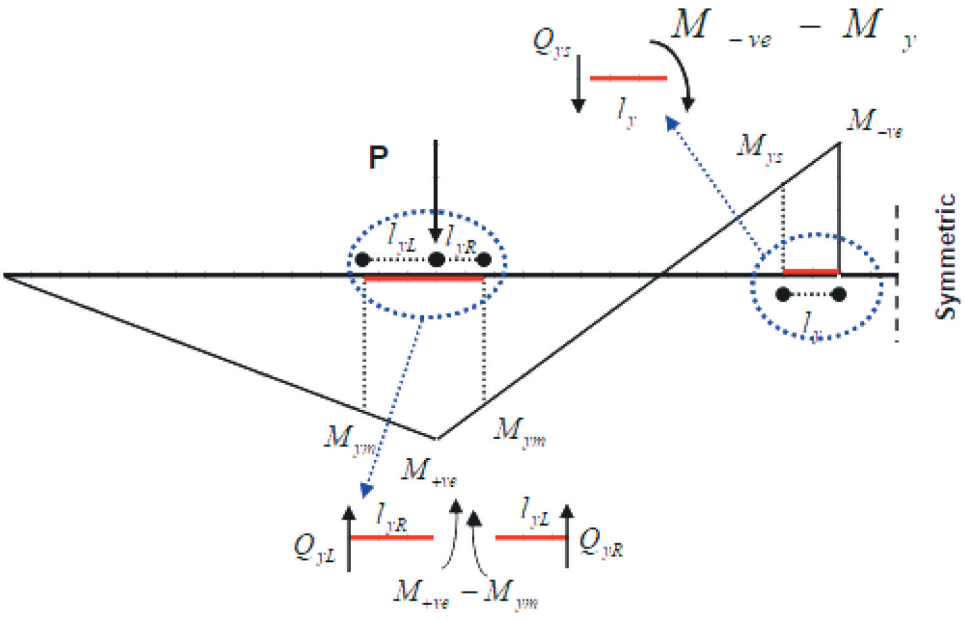

Figure 9. Continuous beam as example for analysing.

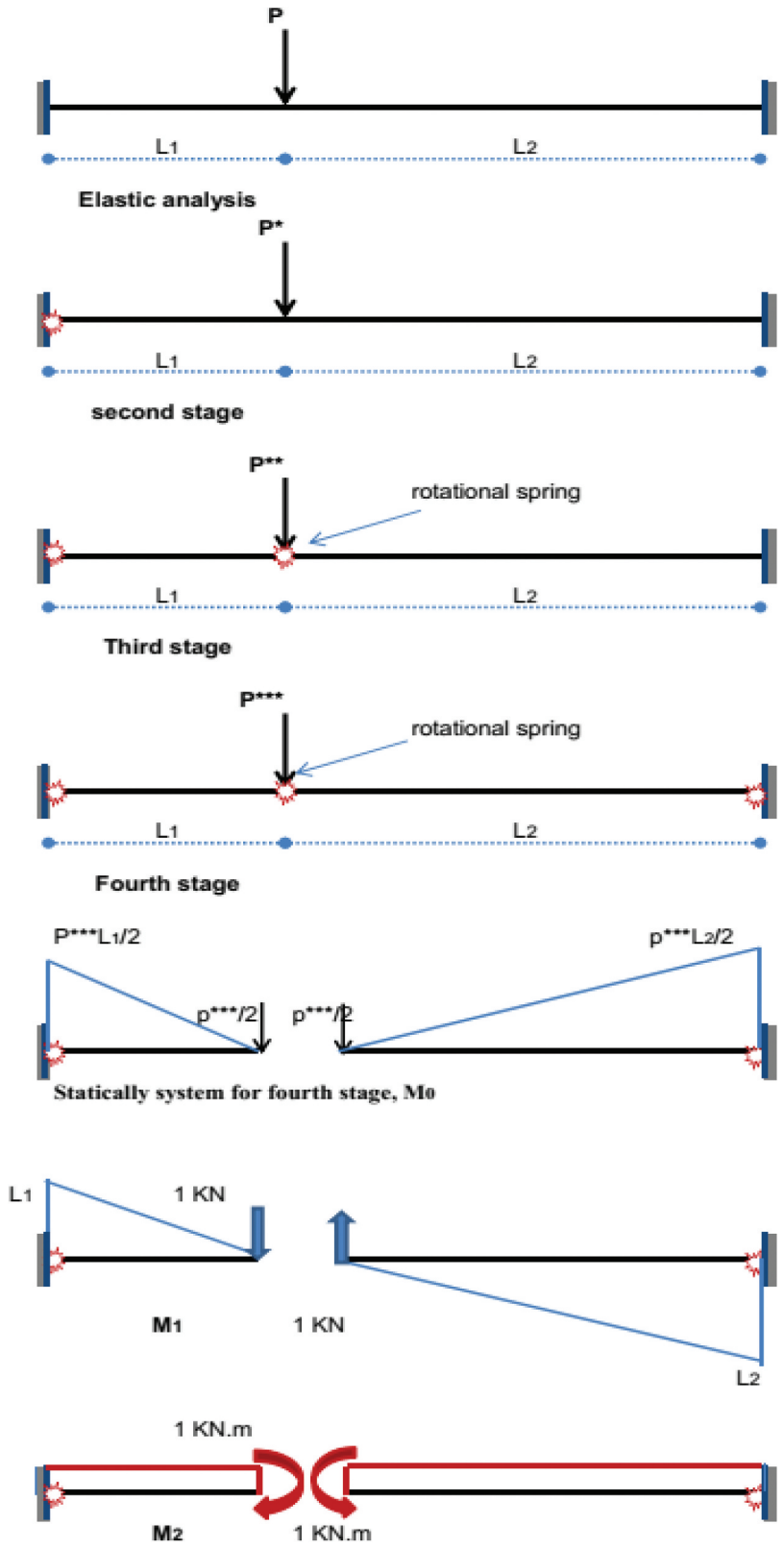

Figure 10. Modelling the virtual beam.

$$l_y = \frac{\Delta M_{-ve}}{P/2 + M_{-ve}/L} \tag{31}$$

By substituting Eq. (31) in Eq. (20), and multiplying the right side of result equation by $\frac{(M_{-ve}-M_y)}{(M_{-ve}-M_y)}\frac{L}{L}$, the equation will as

$$\theta_p = \frac{L}{2}\frac{(\phi_u-\phi_y)}{(M_u-M_y)} \cdot \frac{\Delta M^2{}_{-ve}}{p/2+M_{-ve}/L}\left(\frac{1}{L}\right) \quad \textbf{(32)}$$ it can be put $\frac{1}{K_\theta} = \frac{L}{2}\frac{(\phi_u-\phi_y)}{(M_u-M_y)}$ **(33)**

And,

$$M*_{-ve} = \frac{\Delta M^2{}_{-ve}}{p/2 + M_{-ve}/L}\left(\frac{1}{L}\right) \tag{34}$$

Equation (32) can be transformed to a linear equation as

$$\theta_p = \frac{M*_{-ve}}{K_\theta} \tag{35}$$

whereK_θ, M^*_{-ve} are the spring rotational stiffness at the support and the negative moment in a virtual beam, respectively.

If the yield occurs at the positive moment zone, Eq. (20) will be as

$$\theta_{p(rel)} = \frac{1}{2}(\phi - \phi_y).(l_{yR} + l_{yL}) \tag{36}$$

where $\theta_{p(rel)}$: The relative plastic hinge of the middle section.

l_{yR}, $l_{yL}$are the right and left yield lengths, respectively.

And $l_y$can be determined as

$$M_{+ve} - M_y = \Delta M_{+ve} = Q_R.l_{yR} \tag{37}$$

$$Q_R = \frac{p}{2} + \frac{M_{-ve}}{L} \tag{38}$$

$$l_{yR} = \frac{\Delta M_{+ve}}{P/2 + M_{-ve}/L} \tag{39}$$

Also,

$$M_{+ve} - M_y = \Delta M_{+ve} = Q_L.l_{yL} \tag{40}$$

$$Q_L = \frac{p}{2} - \frac{M_{-ve}}{L} \tag{41}$$

$$l_{yL} = \frac{\Delta M_{+ve}}{P/2 - M_{-ve}/L} \tag{42}$$

By substituting Eqs. (39,42), in Eq. (36) and making the same steps of the negative zone, it can be obtained on the following:

$$\frac{1}{K_{\backslash \text{thetam}}} = \frac{L}{2}\frac{(\phi_u - \phi_y)_m}{(M_u - M_y)_m} \tag{43}$$

K_θ: The rotational stiffness for positive zone

$(\phi_u,\phi_y)_m$: The ultimate curvature and yield curvature of the middle section, respectively.

$(M_u,M_y)_m$: The ultimate moment and yield moment of the middle section, respectively.

$$M*_{+ve} = \frac{\Delta M^2{}_{+ve}}{L}\left(\frac{1}{p/2 + M_{-ve}/L} + \frac{1}{p/2 - M_{-ve}/L}\right) \tag{44}$$

$$\theta_{p(\text{Rel})} = \frac{M*_{+ve}}{K_\theta} \tag{45}$$

where:$K_{\backslash \text{thetam}}$, M^*_{+ve} are the spring rotational stiffness and the positive moment at middle section in a virtual beam, respectively.

From Eqs. (35) and (45), the beam can be transformed after yielding to a virtual beam, and the plastic zones can be represented as a pin connection with rotational spring. The stiffness of these springs can be computed as in **Eqs. (33)** and (43).

3.2. Computing the actual bending moments after yielding

The virtual moments (M*) will be computed by using linear structural analysis. Then, by solving Eqs. (34) and (44), the actual negative and positive moments can be computed as follows:

By solving Eq. (34) for negative zone, the actual moment is determined as

$$M_{-ve} = \frac{-(-2M_y - M*_{-ve}) + \sqrt{(-2M_y - M*_{-ve})^2 - 4(M_y^2 - M^*_{-ve}pL/2)}}{2} \tag{46}$$

And by solving Eq. (44) for positive zone, the actual moment is determined as

$$M_{+ve} = \frac{-(\frac{-2p}{L}M_y + \frac{2p}{L}M^*_{+ve}) + \sqrt{(\frac{-2p}{L}M_y - \frac{2p}{L}M*_{+ve})^2 - 4.(\frac{p}{L} + \frac{4}{L^2}M^*_{+ve})(\frac{p}{L}M_y^2)}}{2(p/L + 4/L^2M^*_{+ve})} \tag{47}$$

Equations (46) and (47) are solutions for Eqs. (34) and (44), and these equations are for a specific case that is symmetric continuous beam consisting of two bays. But if there are several adjacent bays and more than one concentrated load, it is more difficult obtaining similar equations such as in Eq. (46) and (47), because of that the shearing force which is a part of computing the actual negative bending moments depending on these moments. Thus, for more generalisation, the equations can be simplified by computing a part of shearing force that depends on the actual negative moments approximately as follows:

For negative moment zone, computing the shearing force can be simplified as

$$Q = \frac{p}{2} + \frac{(M_{-ve})Initial}{L}$$

where (p/2) is as shearing force for simply supported beam, and $\frac{(M_{-ve})Initial}{L}$is the simplified shearing force due to the negative moment effect. Initial actual moment will be computed by omitting the shearing force due to the negative moment in Eq. (34) as:

$$M*_{-ve} = \frac{\Delta M^2{}_{-ve}}{p/2}\left(\frac{1}{L}\right) \tag{48}$$

$$(M_{-ve})_{initial} = \sqrt{0.5pLM^*_{-ve}} + M_y \tag{49}$$

Eq. (34) becomes as

$$M*_{-ve} = \frac{\Delta M^2{}_{-ve}}{p/2 + (M_{-ve})_{initial}/L}\left(\frac{1}{L}\right) \quad (50)$$

By solving Eq. (50), the actual negative moment can be computed, then by substituting it in Eq.(44), the actual positive moment will be computed as well.

3.3. Computing the bending moments (M*) at yielding zones in the virtual beam

In this section, a fixed beam under concentrated load as shown in Figure 10 will be analysed as a model that can be easily modified to suitable several cases as shown later. Computing the virtual moment in this model will be discussed as an example. The series of plastic hinges formation can be anticipated from the expected elastic moments. It can be assumed in the current evaluation that, the first plastic hinge is formed at the left fixed support and within the increase of load, another two plastic hinges are formed at the middle section under the load and the right fixed support. So, the moments in the element may go through five stages. The elastic stage in the elastic behaviour is the primary degree, the second stage is after forming the plastic hinge at the left support, in this stage, the fixed support will get replaced with a pin support with rotational spring in a virtual beam as shown in Figure 10. The third stage is when the actual moment at the middle section under load reaches the yield, an intermediate hinge with rotational spring will be inserted in the virtual beam. The fourth stage is when a plastic hinge forms at the right fixed support, where the fixed support will get replaced with a pin support with rotational spring. The last stage is when the actual moment on the fixed supports reaches Mu, and the actual moment at the middle section under load increases until reaching Mu in which the failure mechanism is taking place. In this stage, the beam behaves as a simply supported beam. The other stages are when the beam is indeterminate and it can be solved by one of the structural analysis methods such as the force method or finite element method. By assuming that the virtual beam is at the fourth stage, the main system of the beam in the force method is chosen as in Figure 10, and the solution equations will be as follows:

$$\delta_{10} + Q^*_m\delta_{11} + M^*_m\delta_{12} = 0 \quad (51)$$

$$\delta_{20} + Q^*_m\delta_{21} + M^*_m\delta_{12} = \theta_{pm.rel.} = \frac{-M^*_m}{K_{\backslash \text{thetam}}} \quad (52)$$

where:

Q^*_m : Shear force at the middle section of the virtual beam.

M^*_m : The induced moment at the middle section of the virtual beam.

$\theta_{2rel.}$: Relative plastic rotation at middle section.

$$\delta_{10} = \frac{p***}{3EI}(L_1^3 - L_2^3) + p***\left(\frac{L_1^2}{K_{\theta 1}} - \frac{L_2^2}{K_{\theta 2}}\right) \quad (53)$$

where:

$$P** = p_t - p_{3m} \quad (54)$$

P^{***}: The applied load in the virtual beam at fourth stage.

P_{y3}: The load which causes yield moment at the right fixed support.

P_t : The load at any stage after forming right plastic hinge.

$K_{\theta 1}$: The rotational stiffness of spring at left support.

$K_{\theta 2}$: The rotational stiffness of spring at right support.

$$\delta_{11} = \frac{1}{3EI}(L_1^3 + L_2^3) + \left(\frac{L_1^2}{K_{\theta 1}} + \frac{L_2^2}{K_{\theta_2}}\right) \quad (55)$$

$$\delta_{12} = \delta_{21} = \frac{1}{2EI}(L_1^2 - L_2^2) + \left(\frac{L_1}{K_{\theta_1}} - \frac{L_2}{K_{\theta 2}}\right) \quad (56)$$

$$\delta_{20} = \frac{p^{***}}{2EI}(L_1^2 + L_2^2) + p^{***}\left(\frac{L_1}{K_{\theta_1}} + \frac{L_2}{K_{\theta_2}}\right) \quad (57)$$

$$\delta_{22} = \frac{1}{EI}(L_1 + L_2) + \frac{1}{K_{\theta 1}} + \frac{1}{K_{\theta 2}} \quad (58)$$

By substituting Eqs. (53, 55, 56) in Eq. (51), and Eqs. (56,57,58) in Eq. (52) and solving the result equations. The induced internal forces can be determined as

$$M^*_m = \frac{1}{\left(\frac{\delta^2_{12}}{\delta_{11}} - \delta_{22} - \frac{1}{K_{\backslash \text{thetam}}}\right)}\left[\delta_{20} - \frac{\delta_{12}}{\delta_{11}}.\delta_{10}\right] \quad (59)$$

$$Q_m = \frac{\delta_{10}}{\delta_{11}} - \frac{M_m\delta_{12}}{\delta_{11}} \quad (60)$$

$$M^*_L = p^{***}L_1 + Q^*_mL_1 + M^*_m \quad (61)$$

$$M = P^{***}L_2 - Q^*_mL_2 + M^*_m \quad (62)$$

Where:

M^*_L : The moment at the left support in the virtual beam

M^*_R : The moment at the right support in the virtual beam

If the analysis is in another sequence, where the induced moments at the fixed supports exceed the yield moment and the middle moment does not reach the yield, Eqs. (51–52) can be used with the comply with modifications:

$K_{\backslash \text{thetam}}$in Eq. (52) will be equally to "∞", and $\frac{M_m}{K_{\backslash \text{thetam}}}$ **= zero**

3.4. Summary of using the suggested mathematical model

- Finding (ϕ_y,M_y, ϕ_u and M_u) of each section at the support and middle section, let ($\phi_y s$,$M_y s$)be for the section at the support and ($\phi_y m$,$M_y m$) for the middle section.
- Determining yield load which causes yield at the support by elastic structural analysis ($p_y s$).
- Converting the original beam to a virtual beam by inserting rotational spring at the support with linear rotational spring ($K_\theta s = \frac{2(M_u s - M_y s)}{L(\phi_u s - \phi_y s)}$).
- By the increase of load over ($p_y s$), and the applied load on the virtual beam is

($p_s^* = p - p_y s$). The virtual beam will be analysed by the force method or finite element method to obtain the virtual moment (M*).

- By using the following equation

$M_{-ve} = \frac{-(-2M_y - M*_{-ve}) + \sqrt{(-2M_y - M*_{-ve})^2 - 4(M_y^2 - M^*_{-ve})}}{2}$ for simple case as beam in Figure 9 or by solving the approximate simple equation ($M*_{-ve} = \frac{\Delta M^2_{-ve}}{p/2 + (M_{-ve})_{initial}/L}(\frac{1}{L})$) to obtain the actual moment of the original beam. If the yield will be occurred at the middle section before the failure section at the support. In this case, another rotational spring is inserted at this section in the virtual beam, and the same previous steps will be performed.

If the beam in Figure 10 is as another analysed example which is more comprehensive, by assuming that yield will occur firstly at the section of left support, and this section does not reach the ultimate before yield occurring at middle section and the section of right support, respectively. This analysis can be concluded by the flow chart in Figure 11.

where the shown terms in the flow chart are defining as:

$(S.F)_{\text{mod.1}}$: shear force of the yield section at support 1 in the original beam due to the analysis of virtual beam mode.1 and is as $(S.F)_{\text{mod.1}} = \frac{p}{2} + \left(\frac{(M_1)_{initial} - M_3}{L}\right)$.

M_{1act},M_{2act} and M_{3act}: the actual moments after the yield at sections 1,2 and 3, respectively.

M_1^*, M_2^* and M_3^*: the virtual moments at sections 1,2 and 3 in the virtual beam, respectively

$(M_1)_{initial}$: is computed as in Eq. (49)

$(S.F_L)_{\text{mod.2}}$: shear force of yield section at left of concentrated load in the original beam due to the analysis of virtual beam mode.2 and is as $(S.F_L)_{\text{mod.2}} = \frac{p}{2} + \left(\frac{(M_1)_{initial} - M_3}{L}\right)$

$(S.F_R)_{\text{mod.2}}$: shear force of yield section at right of concentrated load in the original beam due to the analysis of virtual beam mode.2 and is as $(S.F_R)_{\text{mod.2}} = \frac{p}{2} - \left(\frac{(M_1)_{initial} - M_3}{L}\right)$.

p_{y1}, p_{y2} and p_{y3}: the load which causes the yield at sections 1, 2 and 3, respectively.

p_t:- the total load at any stage, $p^* = p_t - p_{y1}$, $p^{**} = p_t - p_{y2}$ and $p^{***} = p_t - p_{y3}$.

In fact to make the presented model more comprehensive and valid as well as more easy to apply, the virtual beam can be solved by using finite element method through modifying the stiffness matrix for the beam element according to form of the plastic hinges. The elastic overall matrix of the shown beam in Figure 10 will be modified to fit the different stages of plastic hinges forming as follows:

$$\begin{bmatrix} R_1 \\ M_1 \\ P_2 \\ M_2 \\ R_3 \\ M_3 \end{bmatrix} = \begin{bmatrix} R_1 \\ 0 \\ P^* \\ 0 \\ R_3 \\ M_3 \end{bmatrix} = \begin{bmatrix} v_1 & \theta_1 & v_2 & \theta_2 & v_3 & \theta_3 \\ \frac{12EI}{L_1^3} & \frac{6EI}{L_1^3} & \frac{-12EI}{L_1^3} & \frac{6EI}{L_1^2} & 0 & 0 \\ \frac{6EI}{L_1^3} & \frac{4EI}{L} + K_{\theta 1} & \frac{-6EI}{L_1^3} & \frac{-2EI}{L_1} & 0 & 0 \\ \frac{-12EI}{L_1^3} & \frac{-6EI}{L_1^2} & \frac{12EI}{L_1^3} + \frac{12EI}{L_2^3} & \frac{-6EI}{L_1^2} + \frac{6EI}{L_2^2} & \frac{-12EI}{L_2^3} & \frac{6EI}{L_2^2} \\ \frac{-6EI}{L_1^2} & \frac{-2EI}{L_1} & \frac{-6EI}{L_1^2} + \frac{6EI}{L_2^2} & \frac{4EI}{L_1} + \frac{4EI}{L_2} & \frac{-6EI}{L_2^2} & \frac{-2EI}{L} \\ 0 & 0 & \frac{-12EI}{L_2^3} & \frac{-6EI}{L_2^2} & \frac{12EI}{L_2^3} & \frac{-6EI}{L_2^2} \\ 0 & 0 & \frac{-6EI}{L_2^2} & \frac{-2EI}{L_2} & \frac{-6EI}{L_2^2} & \frac{4EI}{L_2} \end{bmatrix} \begin{bmatrix} v_1 \\ \theta_1 \\ v_2 \\ \theta_2 \\ v_3 \\ \theta_3 \end{bmatrix} \quad (63)$$

In Eqs. (64) and (65), the value of coefficients (α, β)depend on the condition of $v_{2L} = v_{2R}$

3.5. Verification of the suggested mathematical model experimentally

Two series of continuous beams under middle concentrated load were tested by **Chien-Hung Lin *et al.*** (Lin and Chien 2002) to cover investigation of the effect of section ductility on moment redistribution. The details of these beams are shown in Figure 12 and Table 1 . By using the suggested mathematical model, these beams will be analysed and the redistribution moment will be computed and compared to the experimental results.

The stress-strain curve of reinforcement steel of the analysed beams can be simulated by the following equations:

For

$$\varepsilon_s < \varepsilon_y, f_s = (\varepsilon_s/\varepsilon_y) f_y \tag{66}$$

For

$$\varepsilon_y \le \varepsilon_s \le \varepsilon_{sh}, f_s = f_y \tag{67}$$

For

$$\varepsilon_{sh} \le \varepsilon_s \le \varepsilon_{su}, f_s = C_0 + C_1\varepsilon_s + C_2\varepsilon_s^2 + C_3\varepsilon_s^3 + C_4\varepsilon_s^4 \tag{68}$$

where ε_{sh} is the strain at which strain hardening begins andε_u is the ultimate strain. Properties of the reinforcement and the values of the coefficients are shown in Table 2–3 respectively.

The concrete model used in this analysis is based on the concrete modelling in Figure 2

The section was assumed to fail, when the concrete or reinforcement reached the ultimate strain. The following ultimate strain of concrete was used in the numerical analysis (Corley (1966))

$$\varepsilon_{cu} = 0.003 + 0.02(b/z) + (\rho_{sv} f_y/138)^2 \tag{69}$$

ρ_{sv}: the volumetric ratio of reinforcement steel, b: the beam width

z: the distance between the critical section and contraflexure point.

Set A beams were designed to have plastic hinges formed at mid-span (positive moment), while set B beams were designed to be hinged at support point (negative moment). An extra longitudinal reinforcement was added to prevent yielding of the sections outside the predicted hinging area. The virtual beam for the beams of set B can be modelled as the beam in Figure 10, where the beam is considered as fixed at point c and the rotational stiffness at spring support A can be assumed equal to $1E^{-5}$ and the virtual moment can be computed by using Eqs. (59) and (61). The virtual beam model of the beams of set A and the solving equations were built as the same manner. Figures 13–18 show the comparison of the moment-load among the elastic analysis, the suggested mathematical model and the experimental results of the analysed beams.

It was observed from the comparison that the results of the mathematical model after yield are close to the experimental results, where the average differences between them for the all analysed beams do not exceed 5.6%. It seems that computing the moment by the mathematical model after yield is acceptable. Also, it was observed that there is a big gap between the elastic analysis and the results by each of the mathematical model and experimental tests.

4. Degree of moment redistribution

The redistribution of moments may be measured in terms of redistribution defined by

$$\eta = \frac{Mel - Mact}{Mel} \tag{70}$$

In which, *Mel*: elastic moment, *Mact*: actual moment. A reinforced rectangular beam continuous over two equal spans to which two centre-point loads are symmetrically applied at mid span, as shown in Figure 19, this reinforced rectangular beam is used as a reference beam for studying the degree of moment redistribution. The cylinder compressive strength of concrete is taken as 30 MPa. The area of tensile steel over the negative moment region $As2$ varies between 1200 and 6600 mm2, while the ratio $As2/As1$ is fixed at 0.8. For the compressive steel, $As3 = As4 = 600$ mm^2. The yield strength and elastic modulus of steel are taken as 328 MPa and 200 GPa, respectively. The stress–strain curves of the concrete and reinforced steel which are used in this analysis are as shown in Figures 2–3. and the ultimate strain of the concrete is as in Eq. (69).

Figures 20–24 show degree of moment redistribution of the analysed beams.

By using the suggested mathematical model, the degree of the moment redistribution can be computed after yielding to the ultimate stage, not only at the ultimate stage as in the common codes. If assumed according to ACI (ACI Committee 318 2019), Eq.(71), that the studied beams which have reinforcement steel ratio (ρ_s) in-between (0.73–2) %, are under reinforcement. While for the steel ratios 3% and 4%, the beams will be over reinforcement. It was observed for under reinforced beams that degree of moment redistribution of the negative moment is high and it reaches 25%, 18.4% and 16% for beams of ρ_{s2} 0.73%, 1.5% and 2%, respectively.

$$\rho_s \max. = \frac{3\beta_1 f_c^{'}}{8 f_y} \tag{71}$$

While in the over reinforcement beams, degree of moment redistribution for these beams was obviously weak.

The plastic rotation can be computed easily after yield to the ultimate stage by the relationship between it and the moment in the virtual beam ($\theta_p = \frac{M*}{K_\theta}$). Figure 26–30 show the relationship among the plastic rotation, virtual and actual negative moments. The figures illustrate how to transform the nonlinear relationship between the plastic rotation and actual moment to linear relationship between the plastic rotation and virtual moment to ease the analysis.

5. Comparison with code predictions

Four code recommendations are investigated, **EC2** (CEN 2004), **ACI** (ACI Committee 318 2019), **CSA** (CSA 2004) and **BSI (BSI 2007)**. The EC2, ACI and CSA equations were presented in **Eqs. (2), (3) and (4)** respectively. The equation of BSI is as in Eq. (72).

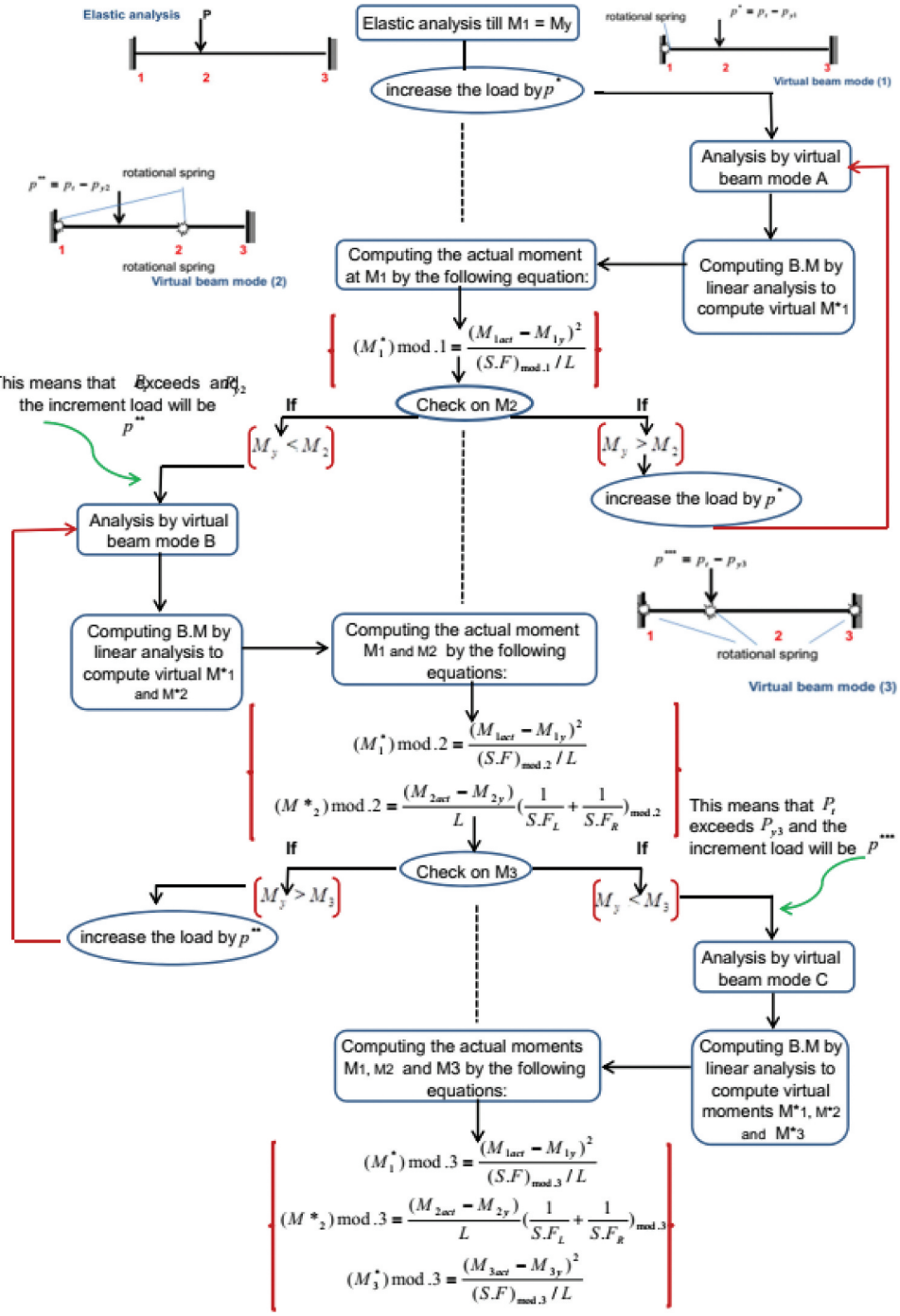

$$(M_1^*)\,\mathrm{mod}.1 = \frac{(M_{1act} - M_{1y})^2}{(S.F)_{\mathrm{mod}.1}/L}$$

$$(M_1^*)\,\mathrm{mod}.2 = \frac{(M_{1act} - M_{1y})^2}{(S.F)_{\mathrm{mod}.2}/L}$$

$$(M^*{}_2)\,\mathrm{mod}.2 = \frac{(M_{2act} - M_{2y})}{L}\left(\frac{1}{S.F_L} + \frac{1}{S.F_R}\right)_{\mathrm{mod}.2}$$

$$(M_1^*)\,\mathrm{mod}.3 = \frac{(M_{1act} - M_{1y})^2}{(S.F)_{\mathrm{mod}.3}/L}$$

$$(M^*{}_2)\,\mathrm{mod}.3 = \frac{(M_{2act} - M_{2y})}{L}\left(\frac{1}{S.F_L} + \frac{1}{S.F_R}\right)_{\mathrm{mod}.3}$$

$$(M_3^*)\,\mathrm{mod}.3 = \frac{(M_{3act} - M_{3y})^2}{(S.F)_{\mathrm{mod}.3}/L}$$

Figure 11. Flow chart for an analysed fixed beam.

$$\eta = 30 - 50\frac{c}{d} \tag{72}$$

The maximum redistribution is 30% for EC2 and BSI while 20% for CSA and ACI. The same beams which were analysed in section (4), will be studied to compare degree of moment redistribution among the suggested mathematical model and code predictions.

Figure 31 and Table 4 show a comparison of the degree of moment redistribution among the suggested mathematical model and the other codes. It was observed the mathematical model gives close results to the results of CSA for studied beams. Also, for ρ_s (2%, 3% and 4%), there was a convergence between the results of ACI and the mathematical model. EC2 and BSI gave far values for the degree of moment redistribution comparing to the mathematical model.

The mathematical model takes into consideration the section geometry, materials properties, reinforcement ratios as well as the effect of the yield length of several zones on the induced moments, while most of the recommended equations by different codes such as EC2 and ACI depended on strains in steel or concrete and section geometry without considering the yield length. So, this may lead to major differences of the results between the mathematical model and the

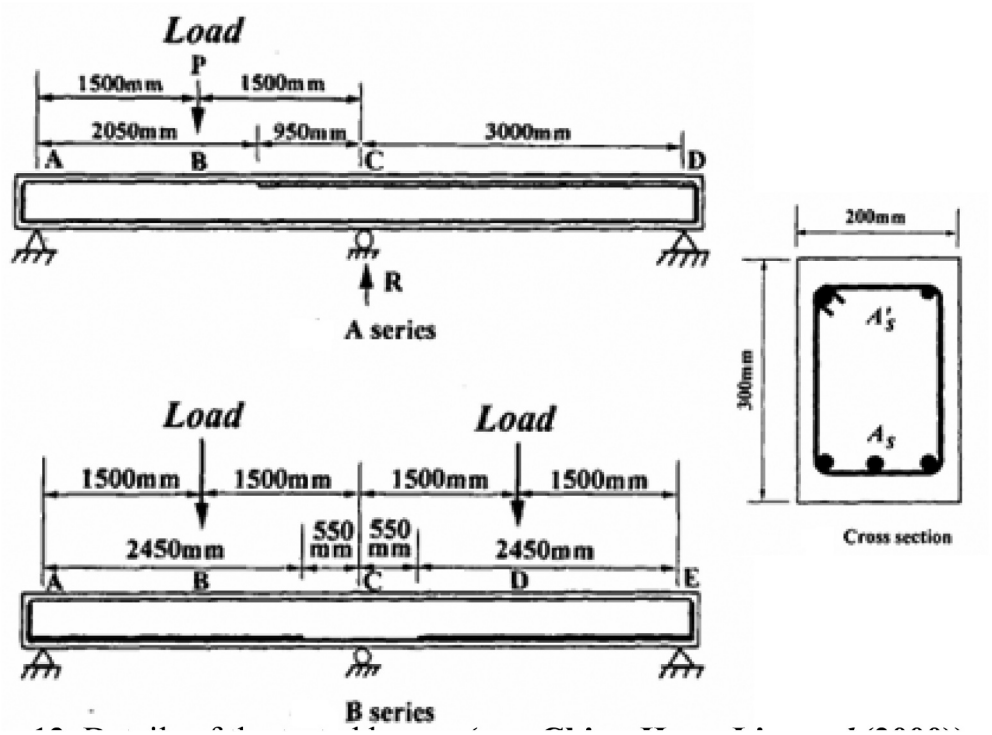

Figure 12. Details of the tested beams **(see Chien-Hung Lin *et al.*(**Lin and Chien 2002)).

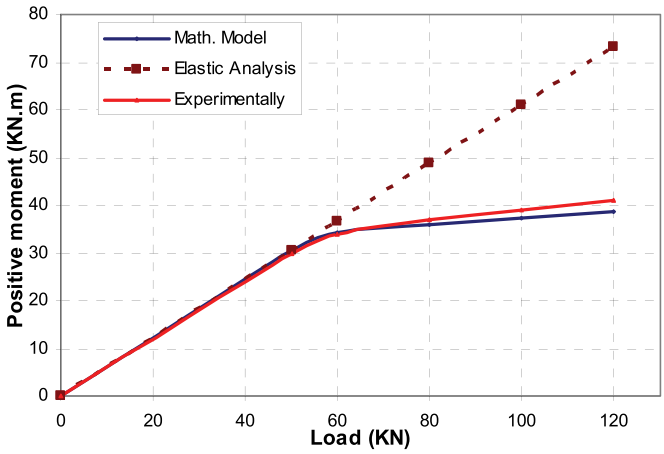

Figure 13. Moment vs. load for beam A1.

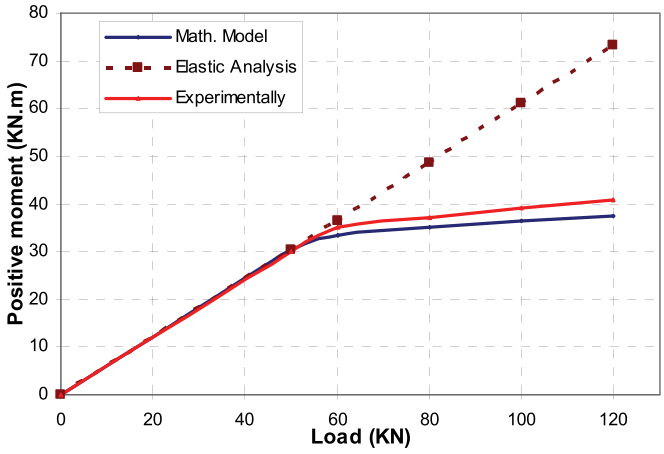

Figure 14. Moment vs. load for beam A5.

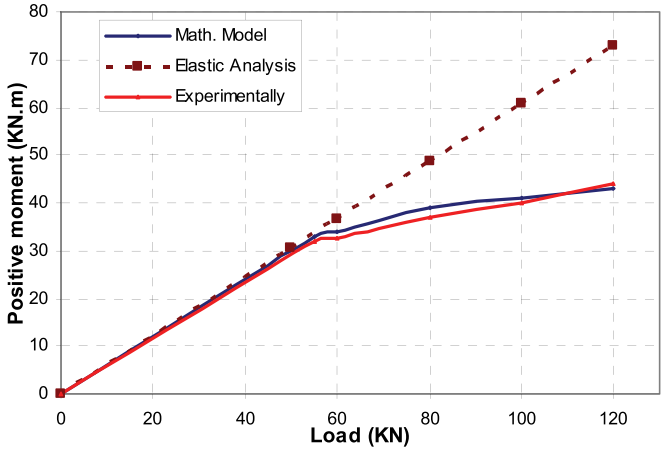

Figure 15. Moment vs. load for beam A11.

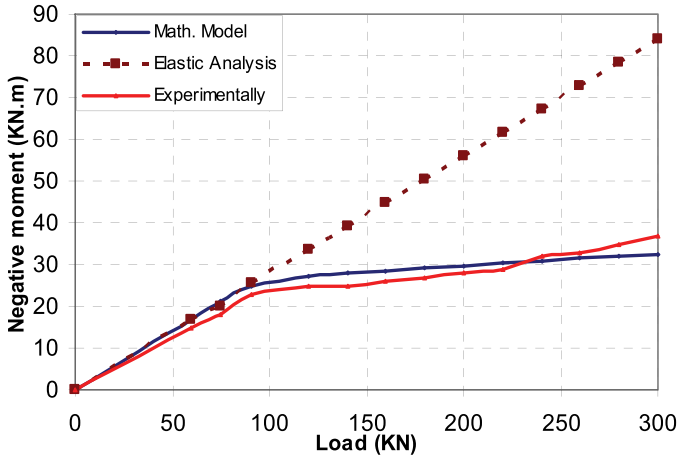

Figure 16. Moment vs. load for beam B2.

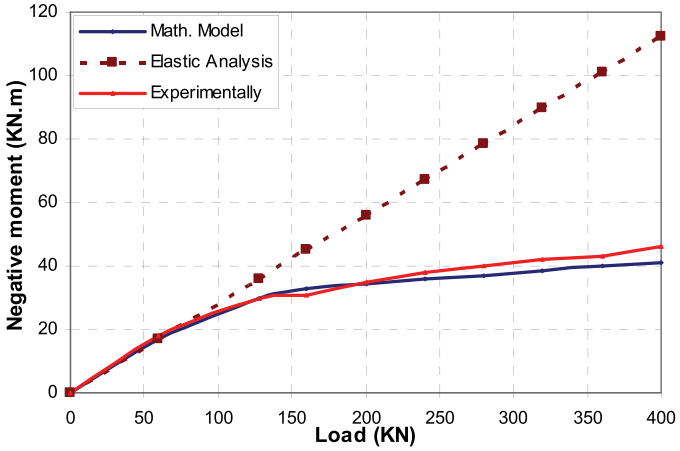

Figure 17. Moment vs. load for beam B5.

different codes, especially for the cases of low reinforcement steel ratio where the moment redistribution is clear.

6. Summary and conclusions

Computing the moments in RC structures after yield needs complicated analysis due to the nonlinear behaviour and linear elastic analysis in this stage can lead to an inaccurate assessment. A mathematical structural model was suggested in this research to compute the moment redistribution and plastic rotations in continuous R.C beams under concentrated load. This model can be used after yielding to the failure stage. The following conclusion has been drawn out of the presented study:

- After yielding, RC beam in the suggested mathematical model is converted into a virtual beam having rotational springs to represent the plastic zones in the original beam. The rotational springs have a constant stiffness in the virtual model to

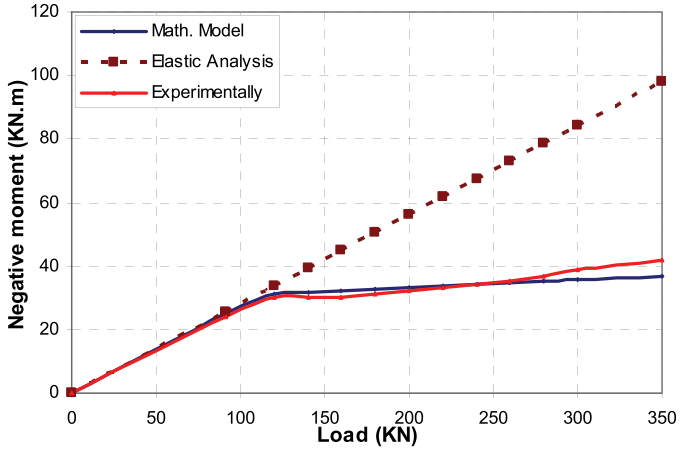

Figure 18. Moment vs. load for beam B12.

Table 1. Details of the analysed beams.

Specimen No.	A_s	$A_s^{'}$	ρ/ρ_b	$\rho\rho\ \rho_b - \rho_b$	$f_c^{'}$	ρ_b
A1	2-#5	2-#3	0.222	0.08	26.5	0.036
A5	2-#5	2-#3	0.231	0.125	25.4	0.034
A11	2-#5	2-#3	0.17	0.061	34.6	0.047
B2	2-#4	2-#3	0.177	0.1	21.2	0.029
B5	2-#5	2-#3	0.277	0.149	21.2	0.029
B12	2-#5	2-#3	0.161	0.058	38.9	0.049

Table 2. Details of reinforcement steel.

#	f_y(Mpa)	ε_y	ε_{sh}	ε_{su}	f_{su}(Mpa)
#3	469	0.00245	0.02283	0.191	667
#4	427	0.00228	0.02650	0.215	604
#5	339	0.00164	0.03638	0.218	471

Table 3. Details of the coefficients.

#	C0	C1	C2	C3	C4
#3	316	9.25E3	−1.03E5	5.35E5	−1.05E6
#4	287	6.93E3	−6.29E4	2.63E5	−4.10E5
#5	173	6.88E3	−6.83E4	3.05E5	−5.07E5

facilitate elastic analysis by one of the linear structural analysis such as (force method). And by presented transformation relationship between the virtual and actual moments, the virtual moment can be computed.

- Based on the approved simplified equation of the plastic rotation capacity in this work which depend on the relationship between the moment and the curvature after yield to the ultimate stage, the mathematical model takes into consideration the section geometry, materials properties, reinforcement ratios as well as the effect of the yielding of several zones on the induced moments.
- The mathematical model was verified experimentally by analysing two tested sets of continuous beams. The results of the mathematical model are close to the experimental results, and the differences between them for all studied beams do not exceed 5.6%.

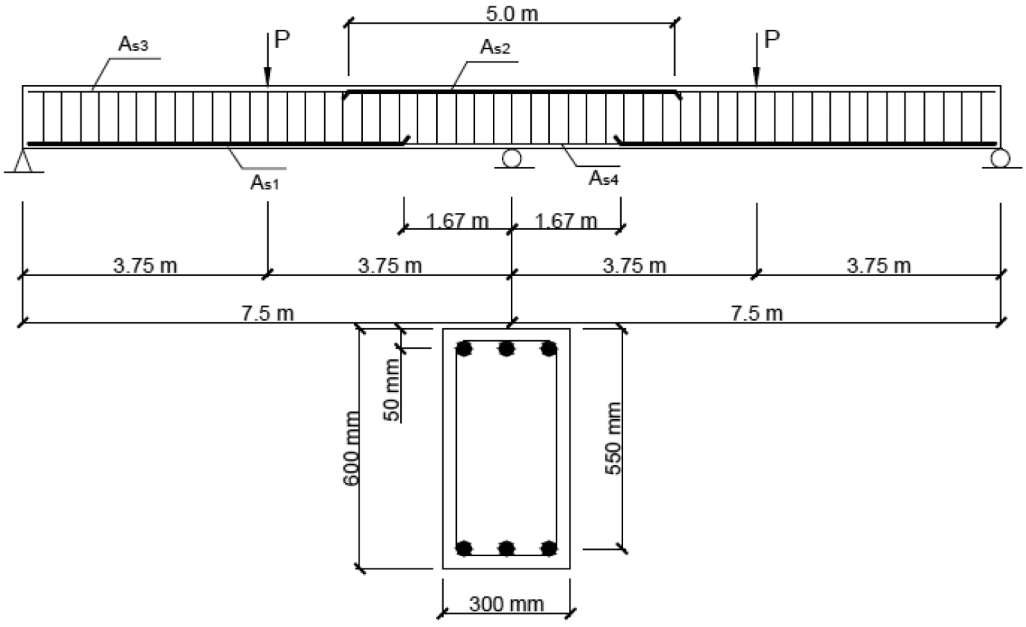

Figure 19. Details of the analysed beam in degree of moment redistribution.

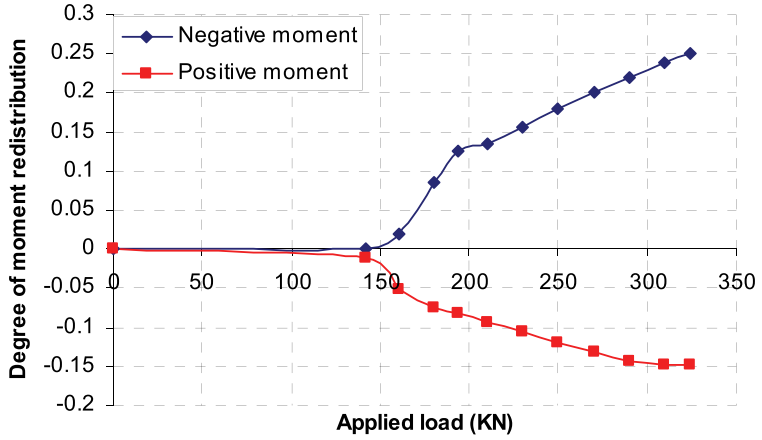

Figure 20. Development of moment.

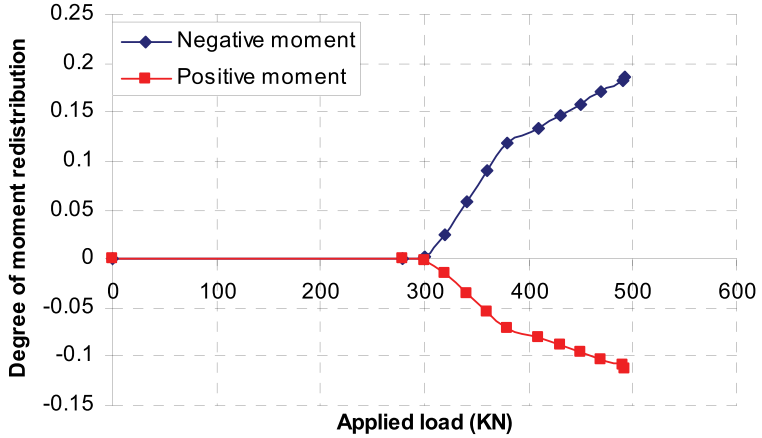

Figure 21. Development of moment redistribution of beam 1(ρ_{s2} =0.73%) redistribution of beam 2(ρ_{s2} =1.5%).

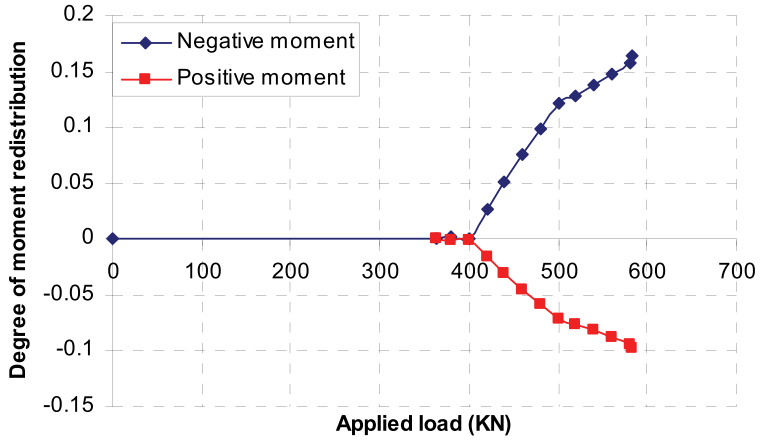

Figure 22. Development of moment.

- A comparison of the degree of moment redistribution among the suggested mathematical model, EC2, ACI, CSA and BSI was performed. The mathematical model gives results close to the results of CSA for the studied beams. Also, for ρ_s (2%, 3% and 4%), there was a convergence between the results of ACI and the mathematical model, but EC2 and BSI gave far values.
- The presented mathematical model for computing the moment redistribution can be developed for more comprehensive and valid as well as more easy to apply by modifying the stiffness matrix of the virtual beam through including the rotational stiffness of springs at plastic zones. Moreover, the approximate following equation

(

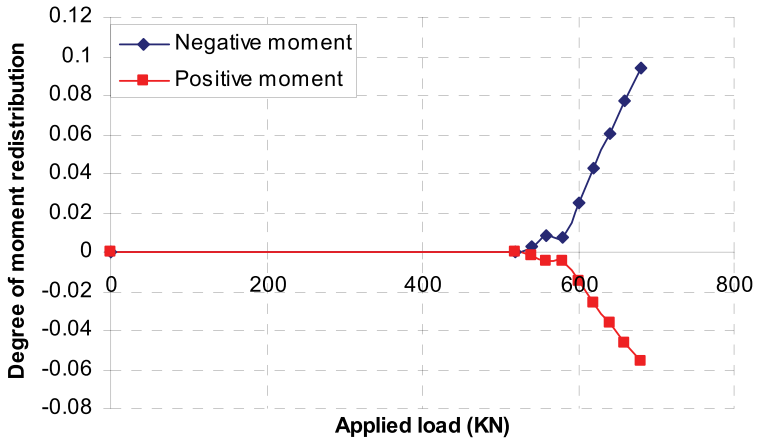

Figure 23. Development of moment redistribution of beam 3(ρ_{s2} = 2%) redistribution of beam 4(ρ_{s2} =3%).

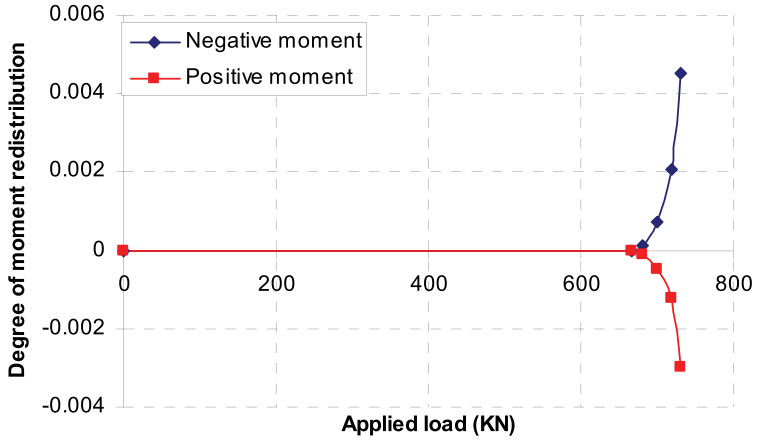

Figure 24. Development of moment Figure 25 degree of moment redistribution of beam 5(ρ_{s2} = 4%) redistribution vs. reinforcement ratioat ultimate load.

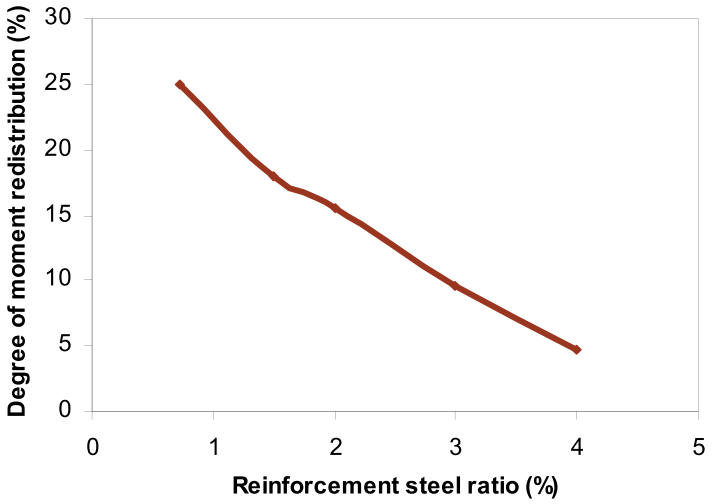

Figure 25. Degree of moment redistribution Vs. reinforcement at ultimate load.

$$M*_{-ve} = \frac{\Delta M^2{}_{-ve}}{p/2 + (M_{-ve})_{initial}/L}\left(\frac{1}{L}\right)$$

for computing actual moments can be used to generalise and facilitate the presented model.

Acknowledgments

We thank our colleagues from Delta University for Since and Technology who provided insight and expertise that greatly assisted the research, although they may not agree with all of the conclusions of this paper.

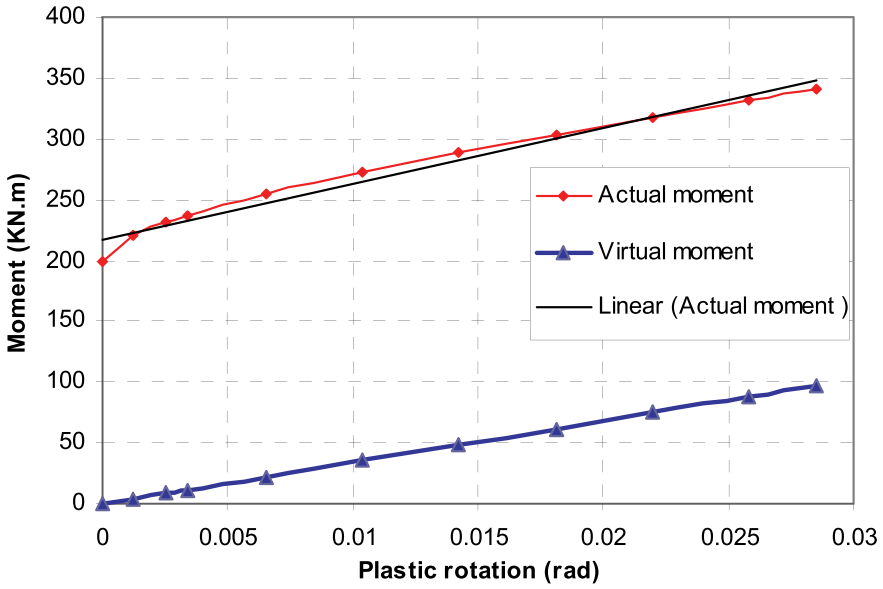

Figure 26. The relationship among actual moment.

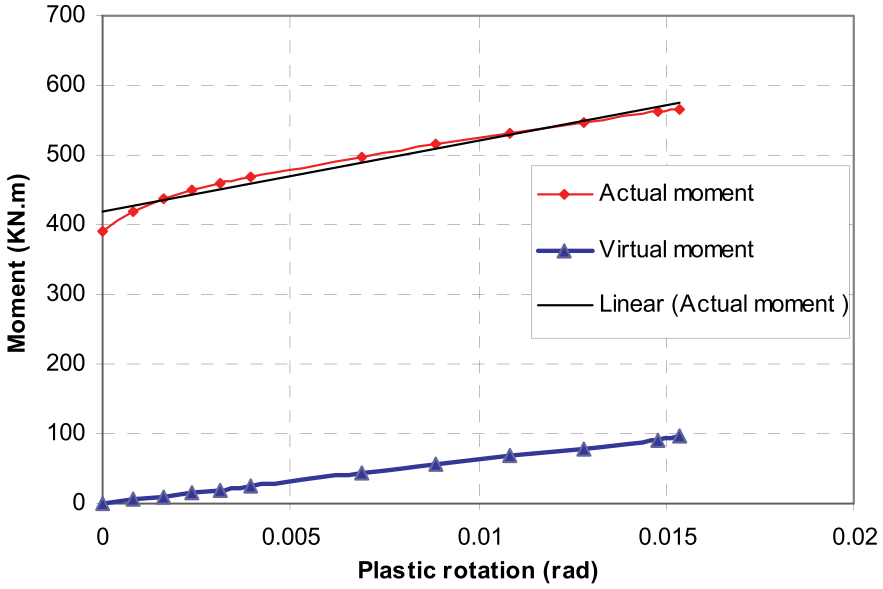

Figure 27. The relationship among actual moment, virtual moment and plastic rotation for, virtual moment and plastic rotation for beam 1(ρ_{s2} = 0.73%) beam 2(ρ_{s2} = 1.5%).

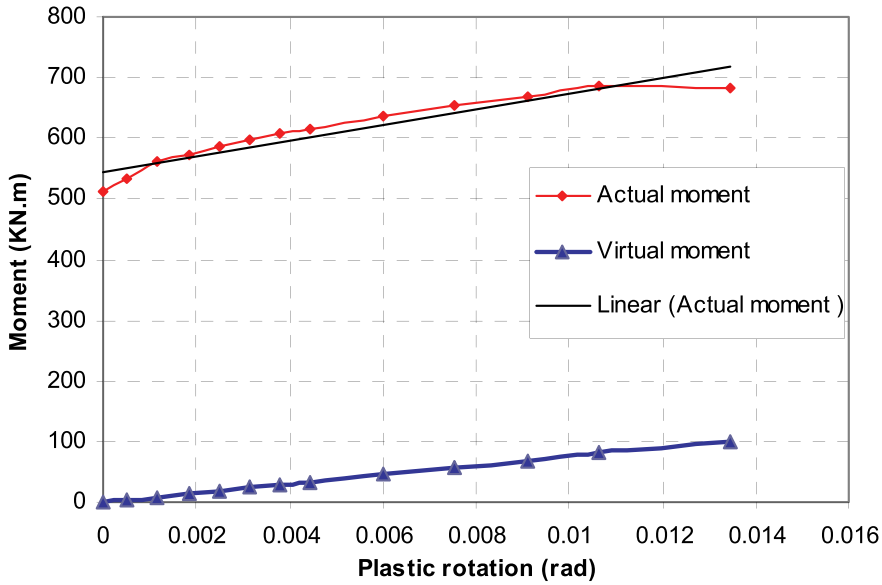

Figure 28. The relationship among actual moment Figure 29 the relationship among actual moment, virtual moment and plastic rotation for, virtual moment and plastic rotation for beam 3(ρ_{s2} = 2%) beam 4(ρ_{s2} = 3%).

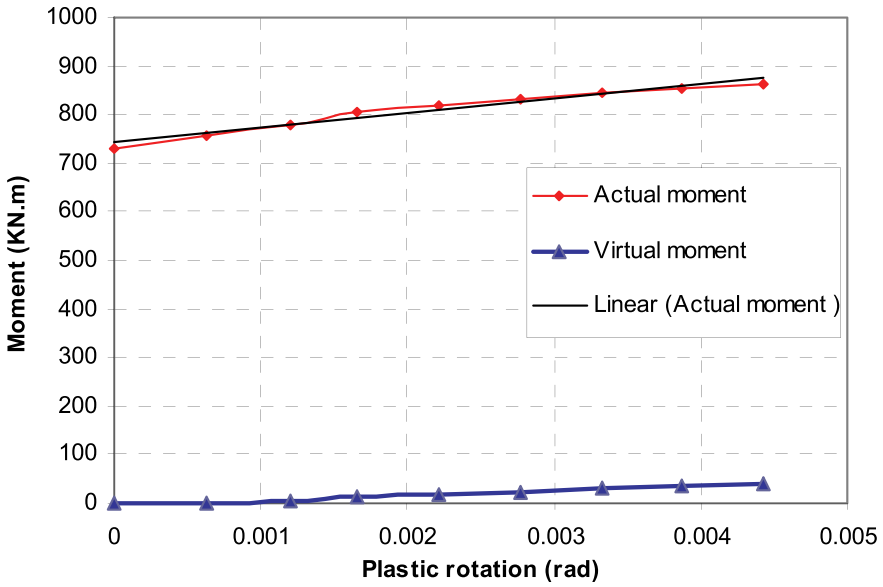

Figure 29. The relationship among actual moment, virtual moment and plastic rotation for beam 4(ρ_{s2} = 3%).

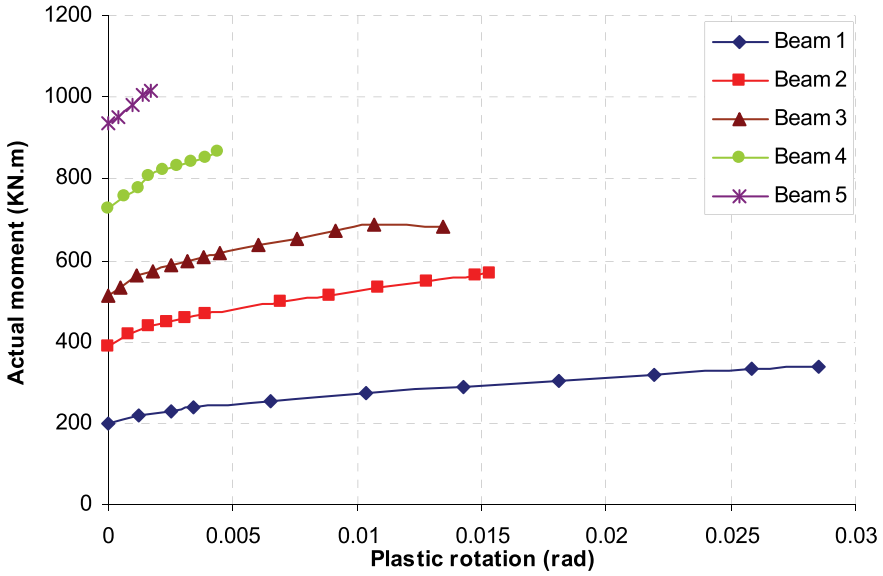

Figure 30. Actual moment vs. plastic rotation for the analysed beams.

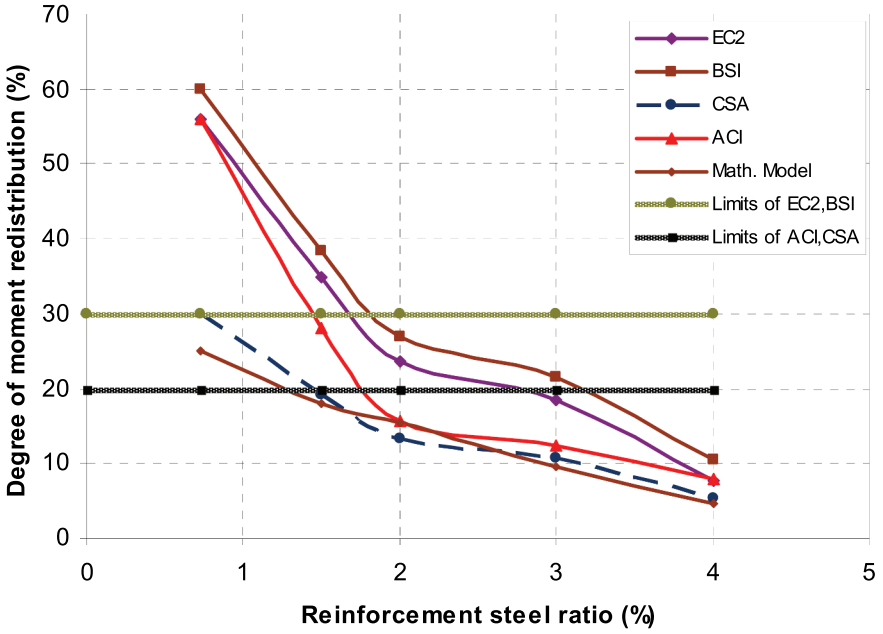

Figure 31. Comparison for degree of moment redistribution among the mathematical model and code predictions.

Table 4. Comparison of degree of moment redistribution among the mathematical model and code predictions.

(ρ_s%)	EC2	BSI	CSI	ACI	Maths. model
0.73	44	47	30	56	25
1.5	34.8	38.32	19.1	28.18	18.4
2	23.7	26.86	13.43	15.74	16
3	18.5	21.5	10.7	12.5	9.3
4	7.8	10.63	5.31	7.99	4.5

We believe these findings will be of interest to the readers of your journal. We declare that this manuscript is original has not been published before and is not currently being considered for publication elsewhere. We know of no conflicts of interest associated with this publication, and there has been no significant financial support for this work that could have influenced its outcome. As corresponding author, I confirm that the manuscript has been read and approved for submission by all named authors.

Disclosure statement

No potential conflict of interest was reported by the author(s).

References

A. Farouk, M., and K. F. Khalil. 2020. "Alternative Mathematical Modeling for Plastic Hinge of Reinforced Concrete Beam." *SN Applied Sciences* 113 (2). 2020. doi:10.1007/S42452-019-1684-9.

ACI Committee 318. 2019. *Building Code Requirements for Structural Concrete (ACI 318–19) and Commentary*. Farmington Hills, MI: American Concrete Institute.

CEB-FIP. 1998. *Ductility of Reinforced Concrete Structures*, Bulletin d'Information. Lausanne: Comité Euro-International du Béton.

CEN. 2004. *Eurocode 2 (EC2): Design of Concrete structures-Part 1–1: General Rules and Rules for Buildings*. EN 1992-1-1. Brussels, Belgium: European Committee for Standardization.

Cohn, M. Z. (1964) "Rotational Compatibility in the Limit Design of Reinforced Concrete Continuous Beams" International Symposium on the Flexural Mechanics of Reinforced Concrete, ASCE-ACI, Miami,359–382.

Corley, W. G. 1966. "Rotation Capacity of Reinforced Concrete Beams." *Proceedings of the ASCE Structural Journal* 92 (ST–4): 121–146.

CSA. 2004. *Design of Concrete Structures*. A23.3-04. Mississauga, Ontario, Canada: Canadian Standards Association.

Gamino, A. L., and T. N. Bittencourt. 2007. "Numerical Evaluation of Plastic Rotation Capacity in RC Beams." *Proc Int Conf Fracture Mech Concr Struct* 665–670.

Kodur, V. K. R., and T. I. Campbell. 1999. "Factor Governing Redistribution of Moment in Continuous Prestressed Concrete Beams." *Structural Engineering and Mechanics* 8 (2): 119–136. doi:10.12989/sem.1999.8.2.119.

Lin, C.-H., and Y.-M. Chien. 2002. "Effect of Section Ductility on Moment Redistribution of Continuousconcrete Beams." *Journal of Chinese Institute of Engineers* 23 (2): 131–141. doi:10.1080/02533839.2000.9670531.

Lou, T., S. M. R. Lopes, and A. V. Lopes. 2013. "Flexural Response of Continuous Concrete Beams Prestressed With External Tendons." *Journal of Bridge Engineering* 18 (6): 525–537. doi:10.1061/(ASCE)BE.1943-5592.0000392.

Lou, T., S. M. R. Lopes, and A. V. Lopes. 2014a. "Flexure of Continuous HSC Beams With External CFRP Tendons: Effects of Fibre Elastic Modulus and Steel Ratio." *Composite Structures* 116: 29–37. doi:10.1016/j.compstruct.2014.05.001.

Lou, T., S. M. R. Lopes, and A. V. Lopes. 2014b. "Evaluation of Moment Redistribution in Normal-strength and High-strength Reinforced Concrete Beams." *Journal of Structural Engineering* 140 (10): 04014072. doi:10.1061/(ASCE)ST.1943-541X.0000994.

Lou, T., S. M. R. Lopes, and A. V. Lopes. 2014c. "Factors Affecting Moment Redistribution at Ultimate in Continuous Beams Prestressed With External CFRP Tendons." *Composites Part B: Engineering* 66: 136–146. doi:10.1016/j.compositesb.2014.05.007.

Mattock, A. H. 1959. "Redistribution of Design Bending Moments in Reinforced Concrete Continuous Beams, Proceedings." *Proceedings of the Institution of Civil Engineers* 13 (1): 35–46. doi:10.1680/iicep.1959.12087.

Rodrigues, E. A., L. M. Osvaldo, T. N. Bittencourt, J. L. A. G. Bitencourt, and P. G. C. Prazeres. 2013. "A Finite Element Approach for Predicting the Ultimate Rotation Capacity of RC Beams." *Proc Int Conf Fracture Mech Concr Concr Struct* 8: 1575–1583.

Saenz, L. P. 1965. "Equation for the Stress-Strain Curve of Concrete in Uniaxial and Biaxial Compression of Concrete." *ACI Journal* 61 (9): 1229–1235.

Scholz, H. 1993. "Contribution to Redistribution of Moments in Continuous Reinforced Concrete Beam." *ACIStruct J* 90 (2): 150–155.

Sheikh, S. A., D. Laine, and C. Y. Cui. 2013. "Behavior of Normal- and High-strength Confined Concrete." *ACI Struct. J* 110 (6): 989–999.